IEEJ Journal of Industry Applications
Vol.8 No.5 pp.820–826 DOI: 10.1541/ieejjia.8.820

Paper

Procedure for Optimization of Interior Permanent Magnet Synchronous Motors with Concentrated Windings by Considering End-Leakage Flux

Katsumi Yamazaki[*a)] Senior Member, Hiroki Narushima[*] Member

(Manuscript received Aug. 8, 2018, revised May 1, 2019)

An optimization procedure is proposed to determine the shapes and orientations of permanent magnets in interior permanent magnet synchronous motors with concentrated armature windings. In the proposed procedure, 2D finite element analysis coupled with the armature voltage equation is used to take into account the leakage flux at the end windings. The end leakage inductance in the equation is determined by 3D finite element analysis in advance. By using this procedure, the rotor shape of the motor can be optimized within a practical computational time. First, the validity of the analysis is confirmed by comparing measured and calculated characteristics of the motor. Then, the optimal shape and orientation of the permanent magnets in the motor are discussed using the results of the proposed optimization procedure. It is revealed that the consideration of the end-leakage flux is indispensable to estimate the characteristics of the motors with concentrated windings whose core length is relatively short as compared to the diameter, particularly under flux weakening control. An optimized rotor that reduces the iron loss at high speeds without considerable deterioration of the other important characteristics is also obtained by the proposed optimization procedure.

Keywords: interior permanent magnet motors, concentrated windings, end-leakage flux, optimization, finite element method

1. Introduction

Interior permanent magnet synchronous motors with concentrated armature windings are widely used for industry applications because of many advantages [(1)–(5)]. In these motors, each armature coil is wound onto one stator tooth. As a consequence, the end windings can be shorter than those of the distributed (overlapping) winding motors. Therefore, this motor is particularly useful to reduce the axial length as compared with the distributed winding motor according to the decrease in the size of the end windings.

On the other hand, one of the disadvantages of these motors is the generation of large rotor losses caused by the wide stator-slot pitch [(3)–(5)]. In Ref. (5), the shapes of stator and rotor of an interior permanent magnet motor with concentrated windings is optimized in order to reduce the magnet eddy current loss by using automatic iterative calculations of 2 dimensional (2D) time-stepping finite element analysis with an optimization method. In this optimization, the amplitude and phase angle of armature current are fixed in each motor designs. However, more practical optimization by considering the actual operating condition is desired for advanced motor designs, in particular, under flux weakening control at high speeds. In this case, the armature current angle is determined according to the maximum inverter voltage. Therefore, for the accurate characteristics estimation, finite element analysis should be iteratively carried out to determine the armature current angle at each motor design. Furthermore, 3 dimensional (3D) finite element analysis is strongly required to estimate the accurate armature voltage because considerable end-leakage flux is generated in the interior permanent magnet motors with concentrated windings, whose core length is relatively short as compared with the diameter. However, the application of the 3D time-stepping finite element analysis to this optimization is practically impossible because it requires vast computational time according to the very large number of iterative finite element analyses to determine both the motor design and the appropriate current angle.

From these viewpoints, we propose an optimization procedure using combination of 2D and 3D finite element analyses. In the proposed method, the end-leakage flux is taken into account in the optimization by coupling 2D finite element analysis and the armature voltage equation including the end-leakage inductance. This inductance is calculated by static 3D finite element analysis in advance under the assumption that the end-leakage inductance is constant with the operating condition and detailed motor designs. In this case, the 3D time-stepping finite element analysis is needless. As a consequence, the iterative calculations to determine the motor design and the appropriate current angle can be carried out within practical computational time.

First, the validity of the finite element analysis and the necessity of the consideration for end-leakage flux are discussed by comparing the measured and calculated characteristics of an interior permanent magnet motor with concentrated windings. Then, the shape and the orientation of the permanent magnets in the interior permanent magnet motor are optimized by the proposed procedure to decrease the loss and to increase the torque.

a) Correspondence to: Katsumi Yamazaki. E-mail: yamazaki.katsumi@it-chiba.ac.jp
* Department of Electrical, Electronics, and Computer Engineering, Chiba Institute of Technology
2-17-1, Tsudanuma, Narashino, Chiba 275-0016, Japan

Table 1. Motor Specification

Phases and poles	3 phases, 16 poles
Maximum rotational speed	7000 r/min
Maximum phase current	330 A
Diameter of stator, Core length	255 mm, 55 mm
Number of stator slot	24 (Concentrated)
Magnet type, Magnetization	Nd-Fe-B, 1.24 T
Thickness of electrical steel sheet	0.35 mm

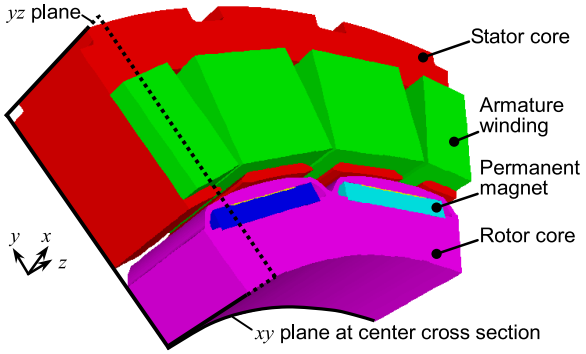

Fig. 1. 3D model of analyzed motor (One pole pair)

2. Analyzed Motor and Calculation Method

2.1 Analyzed Motor Table 1 lists the specification of the initial interior permanent magnet motor. Figure 1 shows the 3D model per pole pair. The motor has one interior magnet per pole. It is a sintered magnet whose remanent flux density is 1.24 T. One magnet is subdivided into 7 pieces along the axial length to prevent the eddy currents. The stator has 24 slots with concentrated windings. Both the stator and rotor cores are laminated. The inverter is an insulated gate bipolar transistor type PWM inverter whose carrier frequency is 10 kHz. In the analysis, the material data is given by the catalogues of the permanent magnet and the electrical steel sheet.

2.2 Proposed Method to Consider End-Leakage Flux Figure 2 shows the flux density distribution calculated by the 3D finite element analysis on the *yz* plane in Fig. 1 under flux weakening control with maximum armature current. The figure indicates considerable flux at the end winding. The 3D analysis is indispensable to estimate this flux. On the other hand, Fig. 3 shows the flux density distribution on the *xy* plane at the center cross section. This distribution can be obtained by both the 2D and 3D finite element analyses. It is observed that the results of the 2D and 3D finite element analyses are nearly identical to each other.

From these results, we propose following method, which approximately estimates the end-leakage flux in the 2D finite element analysis.

1) First, the total armature flux linkage is calculated by both the 3D and 2D finite element analyses, as follows:

$$\Phi_{3D} = \iiint_{V_a} N\boldsymbol{A}\cdot\boldsymbol{n}dv/S_a \quad \cdots\cdots (1)$$

$$\Phi_{2D} = L\iint_{S_a} NA_z n_z dS/S_a \quad \cdots\cdots (2)$$

where Φ_{3D} and Φ_{2D} are the total armature flux linkage calculated by the 3D and 2D finite element analyses, respectively, V_a and S_a are the volume and the cross sectional area of the armature winding, respectively, $\boldsymbol{n}$ and n_z are the unit vector and unit z component that are parallel to the armature current, respectively, $\boldsymbol{A}$ and A_z are the magnetic vector potentials used in the 3D and 2D finite element analyses, respectively, N is the number of armature-winding turns, L is the core length.

2) Then, the end-leakage flux Φ_{end} is defined as the difference between Φ_{3D} and Φ_{2D}, as follows:

$$\Phi_{end} = \Phi_{3D} - \Phi_{2D}. \quad \cdots\cdots (3)$$

3) It is considered that Φ_{end} is mainly produced by the armature current i_a. Therefore, the end-leakage inductance L_e is

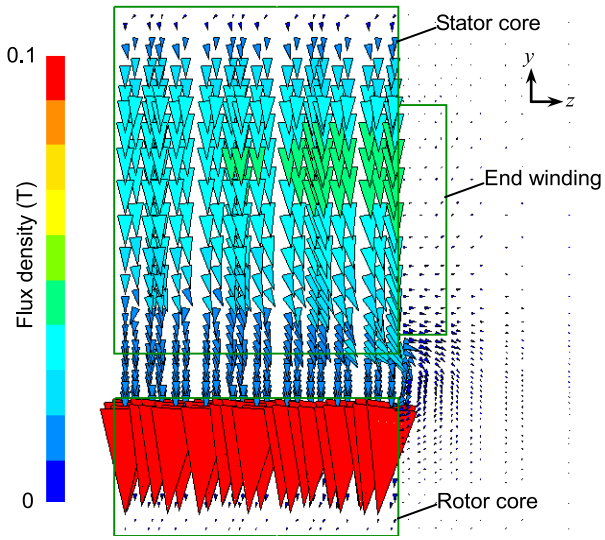

Fig. 2. Flux density distribution on *yz* plane by 3D finite element analysis

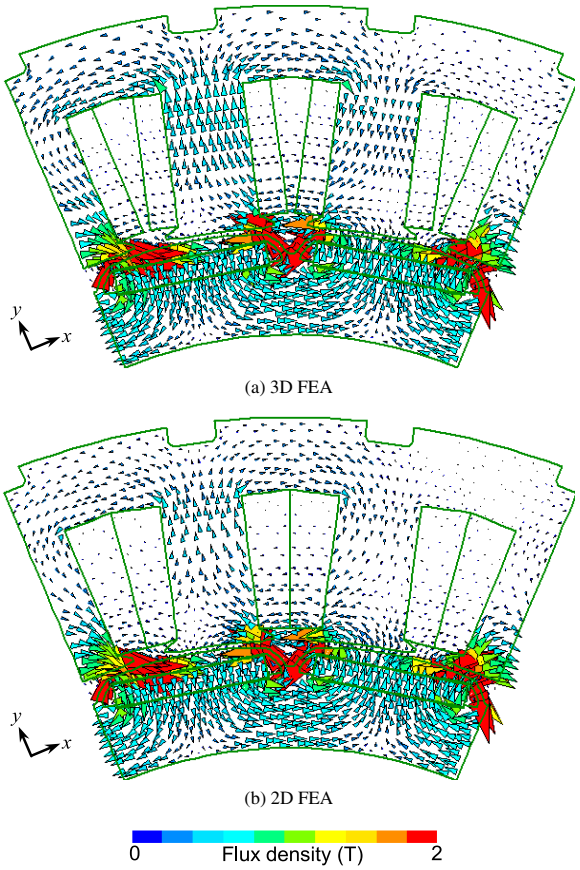

Fig. 3. Flux density distribution on *xy* plane

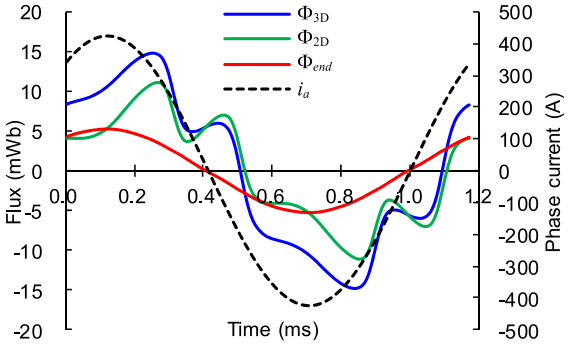

Fig. 4. Time variation in fluxes and armature current

defined, as follows:

$$L_e = \Phi_{end}/i_a \quad \cdots\cdots (4)$$

4) The armature voltage of the motor v_a is estimated by following armature voltage equation including Φ_{2D} and L_e:

$$v_a = \frac{d\Phi_{2D}}{dt} + R_a i_a + L_e \frac{di_a}{dt} \quad \cdots\cdots (5)$$

where R_a is the armature resistance.

Figure 4 shows the calculated time variation in Φ_{3D}, Φ_{2D}, Φ_{end}, and i_a. It is confirmed that Φ_{3D} is larger than Φ_{2D}. In addition, Φ_{end} and i_a show sinusoidal variation with an identical phase, whereas Φ_{3D} and Φ_{2D} are not sinusoidal. This is because Φ_{end} is mainly produced only by i_a, whereas Φ_{3D} and Φ_{2D} are produced by both i_a and residual flux density of the permanent magnets.

As Φ_{end} is nearly proportional to i_a, the end-leakage inductance L_e can be determined by the static solution when i_a is maximum. Therefore, time-stepping 3D finite element analysis is needless. In addition, it is considered that L_e is not considerably affected by the core shape and operating conditions because it is mainly determined by the magnetic resistance at the air region. Therefore, L_e can be fixed in the optimization procedure.

3. Experimental Verification

Next, the validity of the proposed method for end-leakage flux is confirmed by the measurement of initial motor. In the calculation, the amplitude and phase of the armature current are set to be identical to those in the measurement. The end leakage inductance L_e is determined to be 12.23 μH by using the calculated fluxes under the maximum speed condition.

Figure 5 shows the experimental and calculated torque-speed curves when the armature current is 300 A. Both the results of 3D and 2D finite element analyses are found to be in good agreement with the experimental result. The slight overestimation by the calculation must have been caused by the effect of temperature rise of the permanent magnets.

Figure 6 shows the experimental and calculated armature voltages. The result calculated by the 2D finite element analysis without L_e considerably underestimates the armature voltage at the constant voltage region under flux weakening control. It is considered that the ratio of the end-leakage flux to the total flux linkage becomes large under the flux weakening control because only the flux in the core is reduced by the flux weakening. On the other hand, the result of the 2D

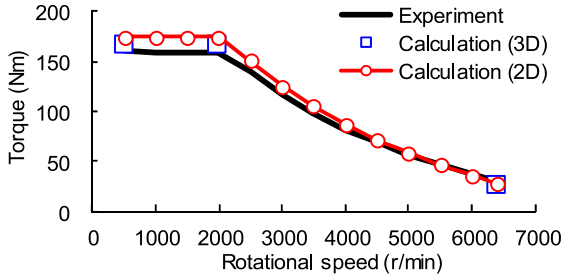

Fig. 5. Experimental and calculated torques (300 A)

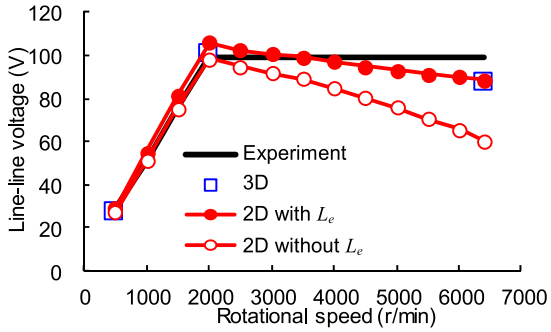

Fig. 6. Experimental and calculated armature voltages (300 A)

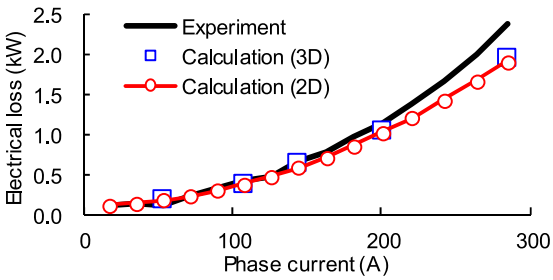

Fig. 7. Experimental and calculated electrical losses (2000 r/min)

finite element analysis with L_e is found to be in good agreement with the result of the 3D finite element analysis and the experiment.

Figure 7 shows the experimental and calculated electrical losses at 2000 r/min under maximum torque control. The stator/rotor core losses and permanent magnet eddy current losses are calculated by the method described in (4). In the 2D finite element analysis, the conductivity of the permanent magnets is modified by Russell and Norsworthy coefficient [5]. The slight underestimation must have been caused by the neglect of the harmonic losses caused by inverter carrier.

From these results, it can be stated that the 2D finite element analysis with the proposed end-leakage inductance gives acceptable results of the motor characteristics.

4. Rotor Magnet Optimization

4.1 Conditions of Optimization The shape and orientation of permanent magnets in the interior permanent magnet motor are automatically optimized by using the proposed procedure.

Figure 8 shows the design variables. The permanent magnet region is subdivided by 6 regions. By expecting the development of permanent magnet technologies in the near future,

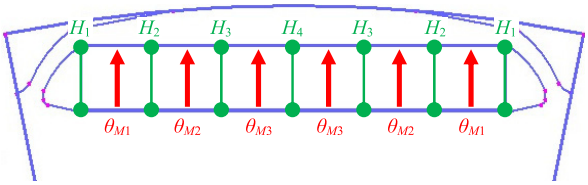

Fig. 8. Design variables for optimization

Table 2. Estimated Driving Conditions

Driving conditions	A : Max torque	B : High speed
Rotational speed (r/min)	500	6000
Armature phase current i_a (A)	330	140
Current angle β (deg)	Peak torque point	Max. voltage point
Line-line voltage V_{line} (V)	Variable	99.0

it is assumed that the magnet orientation can be changed at each region and the shape of the permanent magnet is not restricted to the rectangle. In this case, the design variables are selected, as follows:

1) The orientation (direction of magnetization vector) at each region θ_{M1}, θ_{M2}, and θ_{M3}

2) The position of the permanent magnet surface H_1, H_2, H_3, and H_4

The total magnet volume is set to be constant by moving the bottom position of the permanent magnet according to H_1 to H_4.

Table 2 lists the estimated operating conditions. The condition A is under the maximum torque control, whereas the condition B is under the flux weakening control.

Two optimizations are carried out, as follows:

(a) Maximum torque increase (T_{max} up)

The objective is maximizing the torque T_{max} under the condition A. The constraint condition is imposed on the iron loss (Sum of the core loss and the permanent magnet eddy current loss) W_{iron} under the condition B, which should be less than 105% of the initial motor.

(b) Iron loss reduction at high speeds (W_{iron} down)

The objective is minimizing W_{iron} under condition B. The constraint condition is imposed on the torque T_{max} under the condition A, which should be larger than 97% of the initial motor.

Figure 9 shows the procedure of the optimization. First, the end-leakage inductance L_e is determined due to (1)–(4) by using the 2D and 3D static finite element analyses in advance. As explained in the previous section, this inductance is assumed to be constant with the operating conditions and rotor-design change in the optimization procedure. Rosenbrock's method [5] is selected for the optimization method because this method often gives acceptable results within relatively short computational time. In this method, the design variables are changed alternately and automatically according to the past iterations until the successful design change cannot be found. At each optimization step, the current angle β under the conditions A and B are determined by the iterative calculations of the 2D time stepping finite element analysis. The L_e is not required to search β under the condition A because the torque is not related to L_e when the armature current is given. On the other hand, the L_e is indispensable to search β under the condition B because the armature voltage is considerably affected by L_e, as shown in Fig. 6.

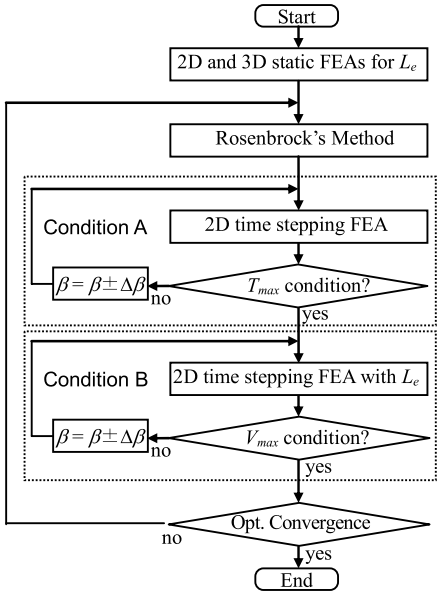

Fig. 9. Procedure of optimization

Table 3. Specification of Optimization Calculation

	T_{max} up	W_{iron} down
Number of optimized iteration	193	102
Average number of elements	7413	6955
Time steps / period	128 step / period	
Total calculation time	122 hour	62 hour
Permissive error coefficient of FEA	10 %	

Core i7 3.5 GHz

Table 4. Calculated Motor Characteristics

		Initial	(a) T_{max} up	(b) W_{iron} down
Angle β (deg)	Con.A	21.3	21.6	14.3
	Con.B	72.7	78.9	69.0
Torque (Nm)	Con.A	188.7	198.6 (+5.2%)	185.4 (-1.8%)
	Con.B	29.9	19.7 (-34.3%)	30.3 (+1.2%)
Iron loss (W)	Con.B	330.7	336.0 (+1.6%)	275.3 (-16.8%)

Table 3 shows the specification of the optimization calculation. An adaptive finite element method with permissive error coefficient [6] is applied to the 2D finite element analyses in order to make the finite element mesh automatically according to the rotor shape determined by Rosenbrock's method.

4.2 Results of Optimization Table 4 lists the characteristics of the initial and optimized motors. Figure 10 shows the variation in shape and orientation according to the optimization iteration.

In the case of the T_{max}-up optimization, the center part of the permanent magnet is shifted to inside of the rotor, whereas the ends of the permanent magnet are shifted to air-gap side. As a consequence, a "partial V-shape" permanent magnet is obtained. The direction of the magnetization vector also inclines to d-axis, particularly at the V-shape part. In this case, the maximum torque increases by 5.2%. This increase is attributed to an increase in the permanent magnet flux by the optimization. However, this flux increase results in a considerable decrease in the torque under the condition B (−34.3%) according to an increase in the current angle β. It can be stated that this motor is not suitable for variable speed

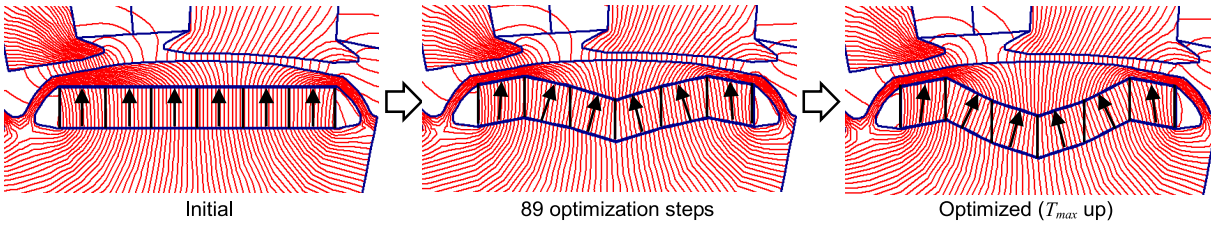

(a) Maximum torque increase (T_{max} up)

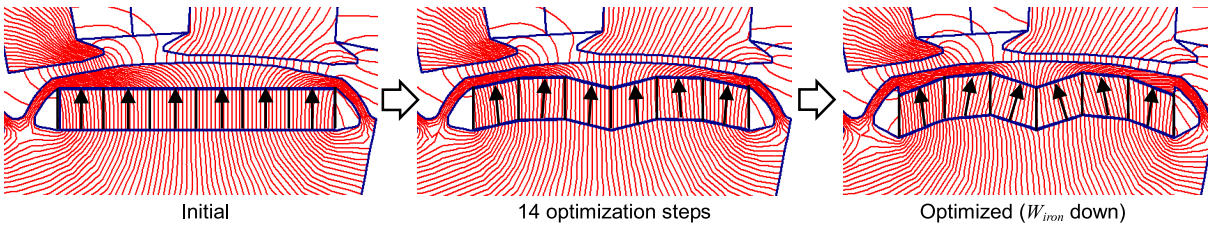

(b) High speed iron loss reduction (W_{iron} down)

Fig. 10. Variation in PM shape and magnetizing direction according to the optimization iterations

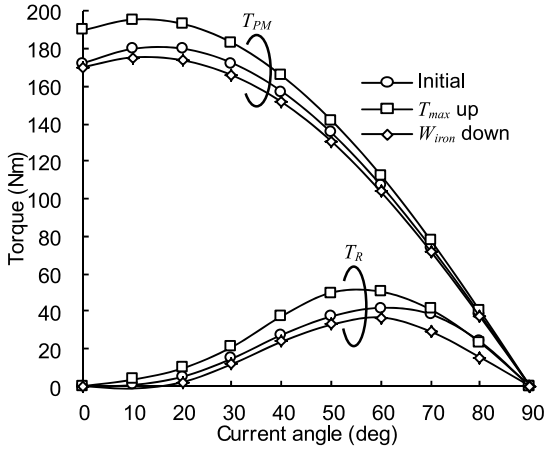

Fig. 11. Calculated magnet and reluctance torques (330 A)

applications.

In the case of the W_{iron}-down optimization, the center part of the permanent magnet is also shifted to inside of the rotor. However, this displacement is smaller than that in the case of the T_{max}-up optimization. The ends of the permanent magnet are also shifted to inside. As a consequence, a "gull-wing" shape permanent magnet is obtained. In this case, the iron loss under the condition B is reduced by −16.8%. In addition, variations in the torque under both the conditions A and B are very small (−1.8% and +1.2%). It can be stated that the iron loss is significantly reduced, whereas the other characteristics are not considerably deteriorated by this optimization.

Figure 11 shows the curves of magnet torque T_{PM} and reluctance torque T_R excluding cross-magnetization components when the armature current is maximum. Both T_{PM} and T_R of the T_{max}-up motor are larger than those of the other motors. However, as mentioned above, too large permanent magnet flux causes the increase in β and decrease in torque under the flux weakening control. On the other hand, the difference between the torque components of the initial motor and those of the W_{iron}-down motors are slight.

4.3 Mechanism of Iron Loss Reduction by Optimization Then, let us discuss why the iron loss is reduced by the W_{iron}-down optimization.

The iron loss of interior permanent magnet motors with 3 slots per pole pair can be classified into following major components [4].

(a) Stator core loss caused by the fundamental rotational field
(b) Stator core losses caused by odd harmonic magnetomotive forces of permanent magnets
(c) Rotor core and permanent magnet losses caused by stator slot harmonics whose order is $3i$ (i is integer)
(d) Carrier harmonic losses caused by inverters.

Figure 12 shows the calculated iron loss components of the initial and optimized motors under the operating condition B. The loss component (d) is neglected because it is not dominant in this condition [4]. The figure indicates that the harmonic loss components (b) and (c) are significantly reduced by the W_{iron}-down optimization.

Figure 13 shows the detailed harmonic loss components. The harmonic stator core losses are significantly reduced by the optimizations. In particular, all the harmonic losses are reduced by the W_{iron}-down optimization. It is considered that the gull-wing shape permanent magnet is very effective to reduce the harmonic magnetomotive forces of permanent magnets. On the other hand, the tendency of the harmonic rotor core losses and permanent magnet eddy current losses are different from each other. The harmonic rotor core losses are also reduced by the optimizations, whereas the harmonic permanent magnet eddy current losses increases, particularly, in the case of the T_{max}-up motor.

To understand these rotor-loss variations, the loss density and permeability distributions under the operating condition B are investigated. Figures 14 and 15 show the results, respectively. Figure 14 indicates that the loss density at the ends of the permanent magnet in the T_{max}-up motor considerably increases. This increase must have been caused by an increase in the slot harmonic effects because the permanent magnet ends were shifted to the air-gap side. On the other hand, the permanent magnet ends of the W_{iron}-down motor

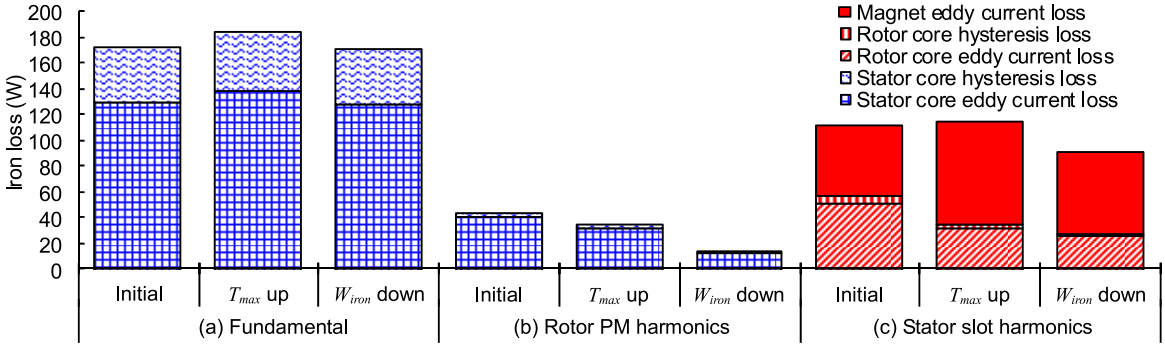

Fig. 12. Iron losses classified according to origins (Driving condition B, High speed, flux weakening)

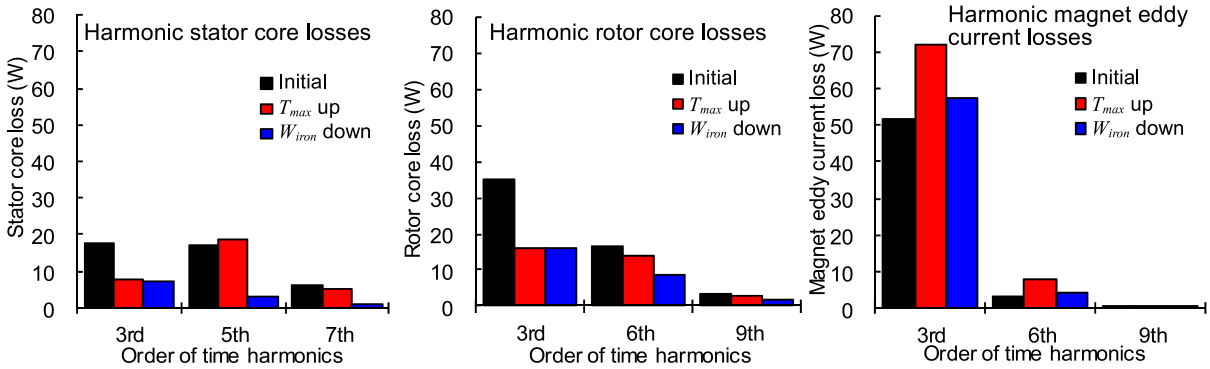

Fig. 13. Calculated harmonic losses (Driving condition B, High speed, flux weakening)

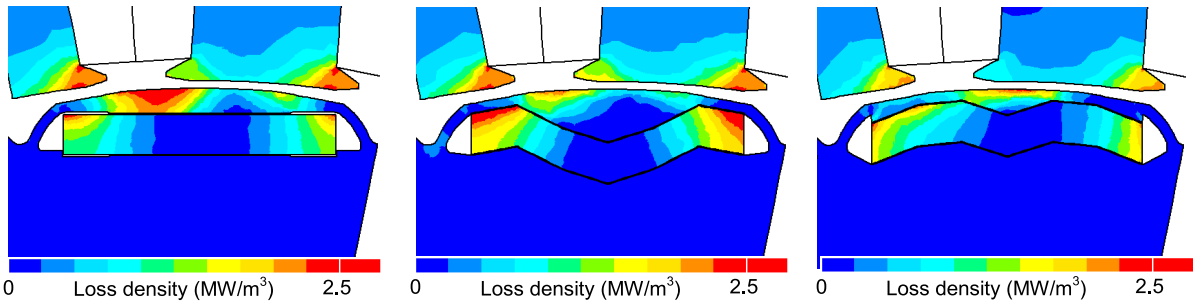

Fig. 14. Loss density distributions (Driving condition B, High speed, flux weakening)

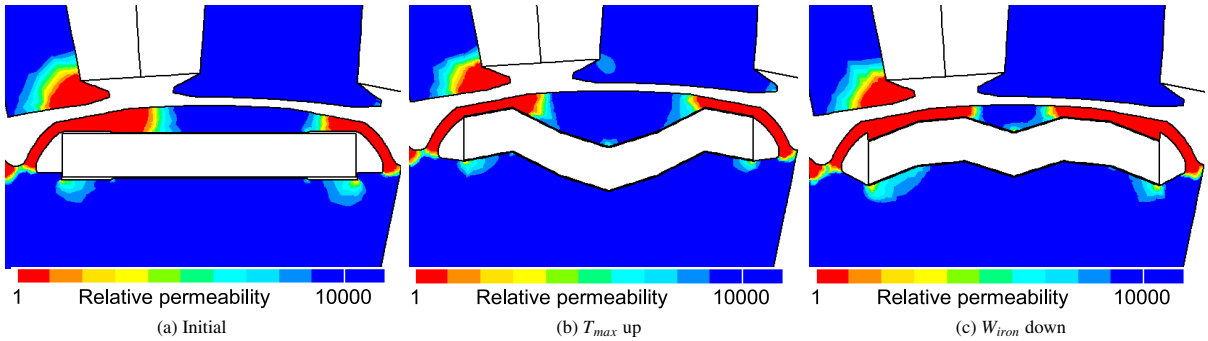

Fig. 15. Calculated permeability distribution (Driving condition B, High speed, flux weakening)

were shifted to inside. As a consequence, the increase in the permanent magnet eddy current loss is suppressed as compared with the T_{max}-up motor. It is also observed that the saturated area at the rotor-core surface increases in the W_{iron}-down motor as compared with the initial and T_{max}-up motor in Fig. 15. As a consequence, the amplitude of the slot harmonic magnetic fields at the rotor surface is reduced in this motor. This is the reason why the harmonic rotor core loss of the W_{iron}-down motor becomes the smallest.

5. Conclusions

A shape optimization procedure that considers the end-leakage flux in interior permanent magnet motors with concentrated windings is proposed. The validity and necessity

of the proposed procedure is confirmed by experimental results. The proposed procedure is applied to the optimization of shape and orientation of rotor permanent magnets by expecting the development of permanent magnet technologies in the near future. Then, a novel rotor design with gull-wing shape permanent magnets, which can reduce the iron loss at high speeds without considerable deterioration of the other characteristics, is obtained. Further work will be required to manufacture the prototype of the optimized motor.

References

(1) J. Cros and P. Viarouge: "Synthesis of high performance PM motors with concentrated windings", *IEEE Trans. on Energy Conversion*, Vol.17, No.2, pp.248–253 (2002)

(2) A.M. El-Refaie, T.M. Jahns, P.J. McCleer, and J.W. McKeever: "Experimental verification of optimal flux weakening in surface PM machines using concentrated windings", *IEEE Trans. on Ind. Appl.*, Vol.42, No.2, pp.443–453 (2006)

(3) S.H. Han, T.M. Jahns, and Z.Q. Zhu: "Analysis of rotor core eddy-current losses in interior permanent magnet synchronous machines", *IEEE Trans. on Ind. Appl.*, Vol.46, No.1, pp.196–205 (2010)

(4) K. Yamazaki, Y. Fukushima, and M. Sato: "Loss analysis of permanent-magnet motors with concentrated windings —variation of magnet eddy current loss due to stator and rotor shapes", *IEEE Trans. on Ind. Appl.*, Vol.45, No.4, pp.1334–1342 (2009)

(5) K. Yamazaki, Y. Kanou, Y. Fukushima, S. Ohki, A. Nezu, T. Ikemi, and R. Mizokami: "Reduction of magnet eddy current loss in interior permanent magnet motors with concentrated windings", *IEEE Trans. Ind. Appl.*, Vol.46, No.6, pp.2434–2441 (2010)

(6) K. Yamazaki, S. Watari, and A. Egawa: "Adaptive finite element meshing for eddy current analysis of moving conductor", *IEEE Trans. Magn.*, Vol.40, No.2, pp.993–996 (2004)

Katsumi Yamazaki (Senior Member) received the B.Eng., M.Eng., and Dr.Eng. degrees from Waseda University, Tokyo, in 1987, 1989, and 1996, respectively. In 1989, he joined the Toshiba Corporation, Tokyo. Since 2007, he has been a professor with Chiba Institute of Technology, Narashino, Japan. His research interests include the analysis and the design optimization of motors. Dr. Yamazaki was the recipient of the Best Poster Paper Awards in IEEE CEFC 2004, ICEM 2006, and IEMDC 2011, respectively. He was a recipient of the 3rd Prize Paper Award of the Electric Machines Committee of the IEEE IAS in 2011 and the Best Paper Award in the IEEE Transactions on Energy Conversion in 2015, respectively.

Hiroki Narushima (Member) received the B.Eng. and M.Eng. degrees from Chiba Institute of Technology, Narashino, Japan in 2016 and 2018, respectively. Now, he is working at Hitachi Automotive Systems, Ltd., Tokyo.